

Distributional Stability of Tangent-Linearized Gaussian Inference on Smooth Manifolds

Junghoon Seo, Hakjin Lee, Jaehoon Sim

Abstract—Gaussian inference on smooth manifolds is central to robotics, but exact marginalization and conditioning are generally non-Gaussian and geometry-dependent. We study tangent-linearized Gaussian inference and derive explicit non-asymptotic W_2 stability bounds for projection marginalization and surface-measure conditioning. The bounds separate local second-order geometric distortion from nonlocal tail leakage and, for Gaussian inputs, yield closed-form diagnostics from (μ, Σ) and curvature/reach surrogates. Circle and planar-pushing experiments validate the predicted calibration transition near $\sqrt{\|\Sigma\|_{\text{op}}}/R \approx 1/6$ and indicate that normal-direction uncertainty is the dominant failure mode when locality breaks. These diagnostics provide practical triggers for switching from single-chart linearization to multi-chart or sample-based manifold inference.

I. INTRODUCTION

Probabilistic inference on smooth manifolds is fundamental in robotics whenever state spaces or constraints are intrinsically nonlinear (e.g., pose/Lie groups [1], contact sets [2, 3], and kinematic manifolds [4]). In these settings, estimators must return both manifold-valued states and calibrated uncertainty for planning, control, and sensor fusion [1]. Two recurring operations are *marginalization* (eliminating nuisance directions) and *conditioning* (enforcing constraints). Although both are classical in Euclidean spaces, their manifold counterparts depend on local geometry and probability-mass locality and are not captured by linear-subspace theory alone [5]. For positive-codimension manifolds, $\{X \in \mathcal{M}\}$ has zero ambient measure; conditioning must therefore be defined by restricting the ambient density to \mathcal{M} and renormalizing with respect to surface measure, rather than by event conditioning in \mathbb{R}^n .

Recently, Guo et al. (2025) [6], the winner of the 2025 IEEE ICRA Best Conference Paper Award, derived explicit Gaussian identities for *linear* constraint manifolds and advocated a linearize–infer–retract workflow for smooth manifolds: linearize at $\tilde{\mu} \in \mathcal{M}$, apply affine-manifold identities on $T_{\tilde{\mu}}\mathcal{M}$, and map the result back to \mathcal{M} using a retraction or chart. In robotics estimation, their framework enables tight, geometry-consistent uncertainty extraction for constrained inference by performing closed-form marginalization/conditioning on tangent-space surrogates and retracting back to the manifold. This viewpoint connects to constrained covariance extraction in factor-graph systems [7], projection-based directional uncertainty models on circles and spheres [8, 9], and geometry-aware filtering on Lie groups/manifolds [10, 11, 12]. Yet the question remains: **when is a single tangent linearization reliable at the distribution level?**

The authors are with AI Robot Team, PIT IN Corp., South Korea. {s|j|h, h|j, s|j|e|h}@pitin-ev.com

In this paper, we formalize reliability as a *distributional* stability question: how close are the exact manifold-induced laws to the laws produced by tangent linearization and retraction? We quantify this discrepancy using the 2-Wasserstein distance W_2 , since it metrizes weak convergence with second moments and therefore directly controls mean and covariance errors [13, 14]. Concretely, for an ambient Gaussian $X \sim \mathcal{N}(\mu, \Sigma)$ and a C^2 embedded submanifold $\mathcal{M} \subset \mathbb{R}^n$, we take as *exact* targets the two canonical ways of pushing mass onto \mathcal{M} :

- **Marginalization via projection:** $P_{\text{marg}} := g_{\#}\mathcal{N}(\mu, \Sigma)$ where g is (locally) the Euclidean metric projection onto \mathcal{M} .
- **Conditioning via surface measure:** P_{cond} with density proportional to the ambient Gaussian density restricted to \mathcal{M} , i.e., $dP_{\text{cond}} \propto \varphi_{\mu, \Sigma} d\text{Vol}_{\mathcal{M}}$. Given a linearization point $\tilde{\mu} \in \mathcal{M}$, its surrogate replaces \mathcal{M} by its tangent space $T_{\tilde{\mu}}\mathcal{M}$, applies the corresponding affine-manifold identities, and then maps the resulting law back to \mathcal{M} via a retraction or chart [6, 15]. Our contributions are threefold:
 - We derive explicit non-asymptotic W_2 stability bounds for projection marginalization and surface-measure conditioning, decomposing error into local second-order geometric distortion and nonlocal tail leakage.
 - We specialize these bounds to Gaussian inputs, yielding computable diagnostics from (μ, Σ) together with local curvature/reach surrogates.
 - We validate the predicted regimes in circle and planar-pushing experiments, including anisotropy, offset, and directional-noise stress tests.

II. PRELIMINARIES

We work in the Euclidean space $(\mathbb{R}^n, \langle \cdot, \cdot \rangle)$ with norm $\|x\| := \sqrt{\langle x, x \rangle}$. For $r > 0$ and $x \in \mathbb{R}^n$, let $B(x, r) := \{z \in \mathbb{R}^n : \|z - x\| \leq r\}$ and $B(r) := B(0, r)$. For a matrix A , $\|A\|_{\text{op}}$ and $\|A\|_F$ denote the operator and Frobenius norms, respectively. We write $\mathbf{1}_A$ for the indicator of an event A . For a measurable map $h : \mathbb{R}^n \rightarrow \mathbb{R}^m$ and a probability measure P on \mathbb{R}^n , the *pushforward* is $h_{\#}P$, defined by $(h_{\#}P)(B) = P(h^{-1}(B))$ for Borel $B \subset \mathbb{R}^m$. If X has law $\mathcal{L}(X) = P$, then $\mathcal{L}(h(X)) = h_{\#}P$.

Wasserstein distance: Let $\mathcal{P}_2(\mathbb{R}^n)$ be the set of Borel probability measures on \mathbb{R}^n with finite second moment. For $P, Q \in \mathcal{P}_2(\mathbb{R}^n)$, the 2-Wasserstein distance [13, 14] is

$$W_2(P, Q) := \inf_{\pi \in \Pi(P, Q)} \left(\int_{\mathbb{R}^n \times \mathbb{R}^n} \|x - y\|^2 d\pi(x, y) \right)^{1/2}, \quad (1)$$

where $\Pi(P, Q)$ denotes the set of couplings of (P, Q) . Equivalently,

$$W_2(P, Q) = \inf \left\{ (\mathbb{E}\|X - Y\|^2)^{1/2} : \begin{aligned} & \mathcal{L}(X) = P, \mathcal{L}(Y) = Q \end{aligned} \right\}. \quad (2)$$

Hence, for any coupling (X, Y) ,

$$W_2(P, Q) \leq (\mathbb{E}\|X - Y\|^2)^{1/2}. \quad (3)$$

If $h : \mathbb{R}^n \rightarrow \mathbb{R}^m$ is L -Lipschitz,

$$W_2(h\#P, h\#Q) \leq L W_2(P, Q). \quad (4)$$

This metric directly serves our goal: deciding when tangent-linearized manifold inference gives reliable first- and second-order uncertainty summaries. For $P, Q \in \mathcal{P}_2(\mathbb{R}^n)$ with means μ_P, μ_Q and uncentered second moments $M_2(P) := \mathbb{E}[XX^\top]$, $M_2(Q) := \mathbb{E}[YY^\top]$, optimal coupling and Cauchy–Schwarz yield

$$\|\mu_P - \mu_Q\| \leq W_2(P, Q), \quad (5)$$

$$\|M_2(P) - M_2(Q)\|_F \leq \sqrt{2(m_2(P) + m_2(Q))} W_2(P, Q). \quad (6)$$

Here $m_2(\nu) := \mathbb{E}_{Z \sim \nu} \|Z\|^2$ for $\nu \in \mathcal{P}_2(\mathbb{R}^n)$. Therefore, W_2 controls both location and second-order discrepancy up to explicit scale factors [16], so we state our main stability results in W_2 as practical calibration criteria for both marginalization and conditioning.

Embedded submanifolds, curvature, and reach: Let $\mathcal{M} \subset \mathbb{R}^n$ be a C^2 embedded submanifold of dimension d . For $y \in \mathcal{M}$, denote by $T_y\mathcal{M}$ its tangent space and by $N_y\mathcal{M} = (T_y\mathcal{M})^\perp$ its normal space. Let $\Pi_{T_y\mathcal{M}}$ and $\Pi_{N_y\mathcal{M}}$ be the corresponding orthogonal projectors. Write $\Pi_y : T_y\mathcal{M} \times T_y\mathcal{M} \rightarrow N_y\mathcal{M}$ for the second fundamental form. The *reach* of a closed set $S \subset \mathbb{R}^n$, $\text{reach}(S)$, is the largest ρ such that every point within distance $< \rho$ has a unique nearest point in S . If $\text{reach}(\mathcal{M}) \geq \rho > 0$, the metric projection g is well-defined on the tube $\mathcal{T}_\rho(\mathcal{M}) := \{x : \text{dist}(x, \mathcal{M}) < \rho\}$ [17].

Retractions and charts: Fix $\tilde{\mu} \in \mathcal{M}$ and write $T := T_{\tilde{\mu}}\mathcal{M}$. A (local) retraction at $\tilde{\mu}$ is a C^2 map $R_{\tilde{\mu}} : B_T(r) \rightarrow \mathcal{M}$ satisfying $R_{\tilde{\mu}}(0) = \tilde{\mu}$ and $DR_{\tilde{\mu}}(0) = \text{Id}_T$. We use a quadratic accuracy bound [15]: there exists $\kappa_R \geq 0$ such that

$$\|R_{\tilde{\mu}}(v) - (\tilde{\mu} + v)\| \leq \frac{\kappa_R}{2} \|v\|^2, \quad \|v\| \leq r. \quad (7)$$

More generally, for a chart $\Psi : B_r \subset \mathbb{R}^d \rightarrow \mathcal{M}$ with $\Psi(0) = \tilde{\mu}$, the induced volume satisfies $d\text{Vol}_{\mathcal{M}}(\Psi(v)) = J(v) dv$ [18].

A. Marginalization and conditioning onto manifolds

Let $X \in \mathbb{R}^n$ have law P with density p , and let $\mathcal{M} = \{x \in \mathbb{R}^n : f(x) = 0\}$ be an m -dimensional smooth manifold defined by a regular map $f : \mathbb{R}^n \rightarrow \mathbb{R}^{n-m}$. Following [6], there are two canonical ways to push probability onto \mathcal{M} : (i) *marginalization by projection*: choose $g_{\mathcal{M}} : \mathbb{R}^n \rightarrow \mathcal{M}$ and set

$$P_{\text{marg}} := (g_{\mathcal{M}})\#P; \quad (8)$$

(ii) *conditioning*: restrict and renormalize, giving

$$dP_{\text{cond}}(x) = Z_{\mathcal{M}}^{-1} p(x) d\text{Vol}_{\mathcal{M}}(x). \quad (9)$$

For $\text{codim}(\mathcal{M}) > 0$, this is *not* event conditioning on $\{X \in \mathcal{M}\}$ (which has measure zero under the ambient law); it is a new probability measure obtained by restricting the density to \mathcal{M} and normalizing with respect to $\text{Vol}_{\mathcal{M}}$.

For an affine linear manifold $\mathcal{M}_{\text{lin}} := \{x \in \mathbb{R}^n : S^\top x = c\}$ with full-rank $S \in \mathbb{R}^{n \times m}$, $m < n$, let N span $\text{null}(S^\top)$ and define $\Pi := N(N^\top N)^{-1}N^\top$. For $X \sim \mathcal{N}(\mu, \Sigma)$, marginalization and conditioning admit closed forms [6]:

$$\mu_{\text{marg}} = \Pi\mu + x_0, \quad \Sigma_{\text{marg}} = \Pi\Sigma\Pi^\top, \quad (10)$$

$$\Sigma_{\text{cond}} = N(N^\top \Sigma^{-1}N)^{-1}N^\top, \quad (11)$$

$$\mu_{\text{cond}} = x_0 + \Sigma_{\text{cond}}\Sigma^{-1}(\mu - x_0),$$

where $x_0 := S(S^\top S)^{-1}c \in \mathcal{M}_{\text{lin}}$.

B. Linearization principle for smooth manifolds

The closed-form identities (10)–(11) hold when the constraint manifold is an affine subspace of \mathbb{R}^n . To extend them to a smooth nonlinear submanifold $\mathcal{M} \subset \mathbb{R}^n$, we adopt a standard *tangent-plane surrogate*: select a linearization point $\tilde{\mu} \in \mathcal{M}$ —typically the Euclidean projection of the ambient mean onto \mathcal{M} or a current estimate—and replace \mathcal{M} locally by its first-order approximation at $\tilde{\mu}$ [6]. Specifically, let $\mathcal{M} = \{x : f(x) = 0\}$ be a regular level set for a smooth $f : \mathbb{R}^n \rightarrow \mathbb{R}^{n-d}$ with $\text{rank } Df(\tilde{\mu}) = n - d$. The tangent space at $\tilde{\mu}$ then admits the affine representation

$$T_{\tilde{\mu}}\mathcal{M} = \{x \in \mathbb{R}^n : S^\top x = c\}, \quad S := Df(\tilde{\mu})^\top, \quad c := S^\top \tilde{\mu},$$

where $N := \text{null}(S^\top)$ spans tangent directions and $\Pi := N(N^\top N)^{-1}N^\top$ is the orthogonal projector onto $T_{\tilde{\mu}}\mathcal{M}$. Applying (10) or (11) in this affine setting yields a *degenerate Gaussian* on $T_{\tilde{\mu}}\mathcal{M}$, constituting a first-order approximation to the on-manifold distribution.

Because tangent-space distributions do not lie on \mathcal{M} itself, the resulting Gaussian is mapped back to \mathcal{M} via a retraction $R_{\tilde{\mu}}$ or an explicit chart Ψ , producing the pushforward $\hat{P} := (R_{\tilde{\mu}})\#P_T$ (or $\hat{P} := \Psi\#Q_T$ in local coordinates), where P_T is the Gaussian on $T_{\tilde{\mu}}\mathcal{M}$. In what follows, we adopt this tangent–retraction construction as the baseline and derive distribution-level error bounds that quantify when a single linearization suffices.

III. W_2 STABILITY FOR GAUSSIAN MARGINALIZATION

Let $\mathcal{M} \subset \mathbb{R}^n$ be a C^2 embedded submanifold and let $X \sim \mathcal{N}(\mu, \Sigma)$ with $\Sigma \succ 0$. With $g : \mathbb{R}^n \rightarrow \mathcal{M}$ denoting a measurable projection map (locally, the metric projection), let $Y := g(X)$ and $P_{\text{marg}} := g\#\mathcal{N}(\mu, \Sigma)$ as in (8). This section quantifies, in W_2 , the discrepancy between P_{marg} and a tangent–retraction surrogate. Given a linearization point $\tilde{\mu} \in \mathcal{M}$, write $T := T_{\tilde{\mu}}\mathcal{M}$ with orthogonal projector Π_T and define

$$\hat{g}(x) := \bar{R}(\Pi_T(x - \tilde{\mu})),$$

$$\hat{Y} := \hat{g}(X),$$

$$\hat{P}_{\text{marg}} := \mathcal{L}(\hat{Y}).$$

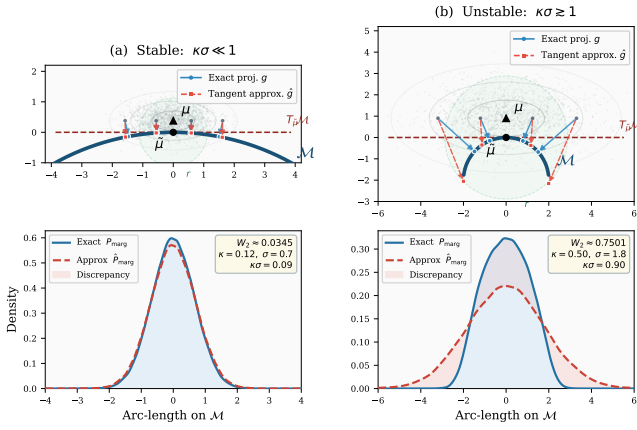


Fig. 1: W_2 stability of marginalizing a Gaussian onto a circular arc. Exact metric projection g vs. the tangent–retraction approximation \hat{g} .

where $\bar{R} : T \rightarrow \mathcal{M}$ is any measurable extension of a local retraction $R_{\tilde{\mu}} : B_T(r) \rightarrow \mathcal{M}$ outside $B_T(r)$. The retraction satisfies the quadratic accuracy bound (7). The main estimate below separates a local second-order geometric error from a tail contribution outside the localization radius r .

Geometric locality: Assume $\text{reach}(\mathcal{M}) \geq \rho > 0$ and fix $r \in (0, \rho/2)$. Under this assumption, g coincides with the unique metric projection on the tube $\mathcal{T}_\rho(\mathcal{M})$. Assume a local curvature bound on $\mathcal{M} \cap B(\tilde{\mu}, 2r)$:

$$\sup_{y \in \mathcal{M} \cap B(\tilde{\mu}, 2r)} \|\Pi_y\|_{\text{op}} \leq \kappa. \quad (12)$$

Theorem III.1 (W_2 stability of marginalization under tangent–retraction). *There exists a constant $C_{\text{loc}} > 0$ (depending only on dimensionless tube/curvature margins, e.g. r/ρ and $r\kappa$, and on the ambient dimension) such that, with $A := \{\|X - \tilde{\mu}\| \leq r\}$ and $\varepsilon := \mathbb{P}(A^c)$,*

$$W_2(P_{\text{marg}}, \hat{P}_{\text{marg}}) \leq C_{\text{loc}}(\kappa + \kappa_R) \left(\mathbb{E}[\|X - \tilde{\mu}\|^4 \mathbf{1}_A] \right)^{1/2} + C_{\text{tail}} \varepsilon^{1/4}, \quad (13)$$

where

$$C_{\text{tail}} := (\mathbb{E}\|Y - \tilde{\mu}\|^4) + (\mathbb{E}\|\hat{Y} - \tilde{\mu}\|^4)^{1/4} < \infty.$$

Remark III.2 (Practical calibration of C_{loc}). *The proof writes C_{loc} as a combination of deterministic local geometry constants (tube-Lipschitz and C^2 graph constants), hence it is independent of (μ, Σ) . A practical recipe is to fix $(r/\rho, r\kappa)$, sample local test points $x_j \in B(\tilde{\mu}, r) \setminus \{\tilde{\mu}\}$, evaluate*

$$\hat{c}_j := \frac{\|g(x_j) - R_{\tilde{\mu}}(\Pi_T(x_j - \tilde{\mu}))\|}{(\kappa + \kappa_R)\|x_j - \tilde{\mu}\|^2},$$

and set C_{loc} to a high quantile of $\{\hat{c}_j\}$ times a safety factor. This makes conservativeness explicit and reproducible.

Proof of Theorem III.1. We couple $Y = g(X)$ and $\hat{Y} = \hat{g}(X)$ through the same Gaussian input X , and we estimate $\mathbb{E}\|Y - \hat{Y}\|^2$ by separating a local region (where geometry is

second-order accurate) from its complement. The deterministic part is a local comparison between metric projection and the tangent–retraction map.

Lemma III.3 (Local quadratic comparison of projection and tangent–retraction). *Under the geometric locality assumptions (Equation (12)), let $R_{\tilde{\mu}} : B_T(r) \rightarrow \mathcal{M}$ be a C^2 retraction with (7). Then there exists $C_{\text{loc}} > 0$ such that for every x with $\|x - \tilde{\mu}\| \leq r$,*

$$\|g(x) - R_{\tilde{\mu}}(\Pi_T(x - \tilde{\mu}))\| \leq C_{\text{loc}}(\kappa + \kappa_R)\|x - \tilde{\mu}\|^2. \quad (14)$$

Proof. Fix x with $d := \|x - \tilde{\mu}\| \leq r$, and define $y := g(x) \in \mathcal{M}$ and $v := \Pi_T(x - \tilde{\mu}) \in T$. Since $r < \rho$, we have $x \in \mathcal{T}_\rho(\mathcal{M})$, so y is well-defined. For sets with reach at least ρ , the metric projection is Lipschitz on $\mathcal{T}_t(\mathcal{M})$ for any $t < \rho$:

$$\text{Lip}(g|_{\mathcal{T}_t(\mathcal{M})}) \leq \frac{\rho}{\rho - t}. \quad (15)$$

Taking $t = r$ and using $g(\tilde{\mu}) = \tilde{\mu}$ gives $\|y - \tilde{\mu}\| \leq \frac{\rho}{\rho - r} d \leq 2d$, hence $y \in \mathcal{M} \cap B(\tilde{\mu}, 2r)$ and (12) applies at y .

Standard C^2 graph estimates on $\mathcal{M} \cap B(\tilde{\mu}, 2r)$ (see, e.g., [19, Lem. 3.2, Lem. 3.5] and [20, Lem. 5.4, Prop. 6.1–6.2]) provide constants $C_{\text{ht}}, C_{\text{ang}} > 0$ such that for all $z \in \mathcal{M} \cap B(\tilde{\mu}, 2r)$,

$$\|\Pi_{T^\perp}(z - \tilde{\mu})\| \leq \frac{C_{\text{ht}}\kappa}{2}\|z - \tilde{\mu}\|^2, \quad (16)$$

$$\|\Pi_{T_z\mathcal{M}} - \Pi_T\|_{\text{op}} \leq C_{\text{ang}}\kappa\|z - \tilde{\mu}\|. \quad (17)$$

Because $y = g(x)$ is a metric projection, $\Pi_{T_y\mathcal{M}}(x - y) = 0$, so

$$\Pi_T(x - y) = (\Pi_T - \Pi_{T_y\mathcal{M}})(x - y).$$

Applying (17) at $z = y$, together with $\|x - y\| \leq d$ and $\|y - \tilde{\mu}\| \leq 2d$, yields

$$\|v - \Pi_T(y - \tilde{\mu})\| \leq 2C_{\text{ang}}\kappa d^2. \quad (18)$$

Likewise, (16) at $z = y$ gives

$$\|\Pi_{T^\perp}(y - \tilde{\mu})\| \leq 2C_{\text{ht}}\kappa d^2. \quad (19)$$

Decomposing $y - (\tilde{\mu} + v) = \Pi_{T^\perp}(y - \tilde{\mu}) + (\Pi_T(y - \tilde{\mu}) - v)$ and combining (18) with (19), we obtain

$$\|y - (\tilde{\mu} + v)\| \leq C_{\text{proj}}\kappa d^2, \quad C_{\text{proj}} := 2(C_{\text{ht}} + C_{\text{ang}}). \quad (20)$$

Finally, (7) and $\|v\| \leq d$ imply

$$\|R_{\tilde{\mu}}(v) - (\tilde{\mu} + v)\| \leq \frac{\kappa_R}{2}d^2,$$

and the triangle inequality between y , $\tilde{\mu} + v$, and $R_{\tilde{\mu}}(v)$ gives (14). \square

Returning to the random setting, the shared-input coupling and (3) give

$$W_2(\mathcal{L}(Y), \mathcal{L}(\hat{Y})) \leq \left(\mathbb{E}\|Y - \hat{Y}\|^2 \right)^{1/2}. \quad (21)$$

Let $A := \{\|X - \tilde{\mu}\| \leq r\}$. Splitting the second moment over A and A^c ,

$$\mathbb{E}\|Y - \hat{Y}\|^2 := \mathbb{E}[\|Y - \hat{Y}\|^2 \mathbf{1}_A] + \mathbb{E}[\|Y - \hat{Y}\|^2 \mathbf{1}_{A^c}]. \quad (22)$$

On A , Lemma III.3 yields

$$\|Y - \widehat{Y}\| \leq C_{\text{loc}}(\kappa + \kappa_R)\|X - \tilde{\mu}\|^2,$$

therefore

$$\begin{aligned} \left(\mathbb{E}[\|Y - \widehat{Y}\|^2 \mathbf{1}_A]\right)^{1/2} &\leq C_{\text{loc}}(\kappa + \kappa_R) \\ &\times \left(\mathbb{E}[\|X - \tilde{\mu}\|^4 \mathbf{1}_A]\right)^{1/2}. \end{aligned} \quad (23)$$

On A^c , by the triangle inequality, $\|Y - \widehat{Y}\| \leq \|Y - \tilde{\mu}\| + \|\widehat{Y} - \tilde{\mu}\|$. Setting $Z := \|Y - \tilde{\mu}\| + \|\widehat{Y} - \tilde{\mu}\|$, we get $\|Y - \widehat{Y}\|^2 \mathbf{1}_{A^c} \leq Z^2 \mathbf{1}_{A^c}$, and Hölder yields

$$\left(\mathbb{E}[\|Y - \widehat{Y}\|^2 \mathbf{1}_{A^c}]\right)^{1/2} \leq \left(\mathbb{E}[Z^4]\right)^{1/4} \varepsilon^{1/4}. \quad (24)$$

By Minkowski's inequality in L^4 ,

$$\left(\mathbb{E}[Z^4]\right)^{1/4} \leq \left(\mathbb{E}\|Y - \tilde{\mu}\|^4\right)^{1/4} + \left(\mathbb{E}\|\widehat{Y} - \tilde{\mu}\|^4\right)^{1/4} =: C_{\text{tail}},$$

so

$$\left(\mathbb{E}[\|Y - \widehat{Y}\|^2 \mathbf{1}_{A^c}]\right)^{1/2} \leq C_{\text{tail}} \varepsilon^{1/4}. \quad (25)$$

Combining (21), (22), (23), and (25) yields (13). \square

Gaussian specialization: Set $\delta := \mu - \tilde{\mu}$ and write $X - \tilde{\mu} = \delta + \xi$ with $\xi \sim \mathcal{N}(0, \Sigma)$. Then the *untruncated* fourth moment in (13) has the closed form

$$\mathbb{E}\|X - \tilde{\mu}\|^4 = \|\delta\|^4 + 2\|\delta\|^2 \text{tr} \Sigma + 4\delta^\top \Sigma \delta + (\text{tr} \Sigma)^2 + 2\|\Sigma\|_F^2. \quad (26)$$

On the localization event

$$A := \{\|X - \tilde{\mu}\| \leq r\},$$

the *localized* fourth moment obeys the explicit bound

$$\mathbb{E}[\|X - \tilde{\mu}\|^4 \mathbf{1}_A] \leq r^4,$$

and can be sharpened by evaluating the CDF of the noncentral quadratic form $\|X - \tilde{\mu}\|^2$ (noncentral χ^2 in the isotropic case).

For the tail probability $\varepsilon := \mathbb{P}(A^c)$, let $\lambda_{\max} := \|\Sigma\|_{\text{op}}$ and $Z \sim \mathcal{N}(0, I_n)$. Using $\mathbb{P}(\|Z\| \geq \sqrt{n} + t) \leq e^{-t^2/2}$ [21] yields, for any $r > \|\delta\|$,

$$\varepsilon = \mathbb{P}(\|X - \tilde{\mu}\| > r) \leq \exp\left(-\frac{1}{2}\left(\frac{r - \|\delta\|}{\sqrt{\lambda_{\max}}} - \sqrt{n}\right)_+^2\right). \quad (27)$$

Equivalently, choosing

$$r = \|\delta\| + \sqrt{\lambda_{\max}}(\sqrt{n} + t) \implies \varepsilon \leq e^{-t^2/2}.$$

Finally, the constant C_{tail} in (13) can be made explicit under mild global extensions. For example, on the tube $\mathcal{T}_r(\mathcal{M})$ with $r < \rho$, the metric projection is Lipschitz with $\text{Lip}(g) \leq \rho/(\rho - r)$, hence

$$\left(\mathbb{E}\|Y - \tilde{\mu}\|^4\right)^{1/4} \leq \left(\frac{\rho}{\rho - r}\right) \left(\mathbb{E}\|X - \tilde{\mu}\|^4\right)^{1/4}.$$

Moreover, the retraction accuracy (7) implies (for $v = \Pi_T(X - \tilde{\mu})$)

$$\begin{aligned} \|\hat{g}(X) - \tilde{\mu}\| &= \|\bar{R}(v) - \tilde{\mu}\| \\ &\leq \|v\| + \frac{\kappa_R}{2} \|v\|^2 \\ &\leq \|X - \tilde{\mu}\| + \frac{\kappa_R}{2} \|X - \tilde{\mu}\|^2, \end{aligned}$$

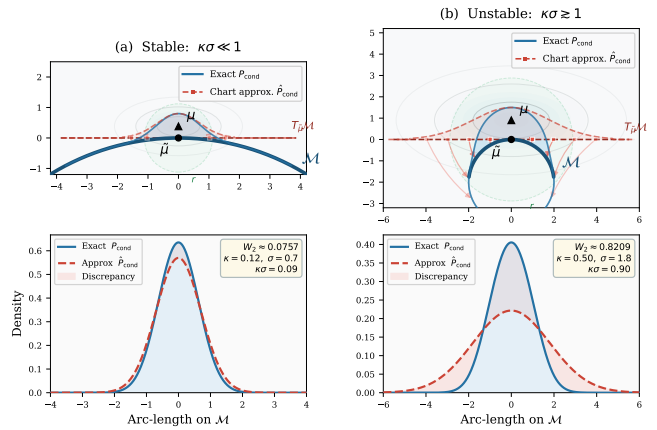


Fig. 2: W_2 stability of conditioning a Gaussian onto a circular arc. Surface-measure conditioning vs. a tangent-plane chart approximation.

so $\mathbb{E}\|\hat{g}(X) - \tilde{\mu}\|^4 < \infty$ and can be bounded by Gaussian moments of order up to 8 when a fully explicit C_{tail} is needed. Substituting these quantities into (13) gives a computable (conservative) criterion in terms of (μ, Σ) and locality parameters $(\rho, \kappa, \kappa_R, r)$.

Interpretation and numerical illustration: Equation (13) decomposes the error into a local geometric term and a tail-leakage term. Inside $A = \{\|X - \tilde{\mu}\| \leq r\}$, the mismatch between g and \hat{g} is second order, scaling as $(\kappa + \kappa_R)\|X - \tilde{\mu}\|^2$ (Lemma III.3). For Gaussian inputs, the effective spread scale is $\|\delta\| + \sqrt{\lambda_{\max}}\sqrt{n}$, so the local term is roughly $(\kappa + \kappa_R)(\|\delta\| + \sqrt{\lambda_{\max}}\sqrt{n})^2$. The tail term is controlled by $\varepsilon = \mathbb{P}(\|X - \tilde{\mu}\| > r)$ and decays exponentially once $r \gtrsim \|\delta\| + \sqrt{\lambda_{\max}}(\sqrt{n} + t)$, but can dominate when reach forces small r . Hence, r must balance probability-mass coverage against local geometric validity. Figure 1 supports this prediction: in local regimes, the exact and approximate laws nearly coincide; beyond the transition, linearization becomes miscalibrated and typically overconfident.

IV. W_2 STABILITY FOR GAUSSIAN CONDITIONING

Let $\mathcal{M} \subset \mathbb{R}^n$ be a C^2 embedded submanifold of dimension d and $X \sim \mathcal{N}(\mu, \Sigma)$ with density $\varphi_{\mu, \Sigma}$. This section quantifies, in W_2 , the discrepancy between the exact conditioned law P_{cond} from (9) (with $\varphi = \varphi_{\mu, \Sigma}$) and an approximation that first conditions on $T_{\tilde{\mu}}\mathcal{M}$ and then maps back to \mathcal{M} through a local chart.

Tangent-plane reference law: Fix $\tilde{\mu} \in \mathcal{M}$ and let $T := T_{\tilde{\mu}}\mathcal{M}$ as in Section III. Let $N \in \mathbb{R}^{n \times d}$ have orthonormal columns spanning T and define the affine parametrization $x_{\text{lin}}(v) = \tilde{\mu} + Nv$ for $v \in \mathbb{R}^d$. Let $\Omega := \Sigma^{-1}$ denote the precision matrix, and recall $\delta = \mu - \tilde{\mu}$ from Section III. Define the probability measure Q_T on \mathbb{R}^d by

$$\begin{aligned} dQ_T(v) &:= \frac{\varphi_{\mu, \Sigma}(\tilde{\mu} + Nv)}{Z_T} dv, \\ Z_T &:= \int_{\mathbb{R}^d} \varphi_{\mu, \Sigma}(\tilde{\mu} + Nv) dv \in (0, \infty). \end{aligned} \quad (28)$$

Equivalently, $Q_T = \mathcal{N}(m_T, \Sigma_T)$ with

$$\Sigma_T = (N^\top \Omega N)^{-1}, \quad m_T = \Sigma_T N^\top \Omega \delta. \quad (29)$$

Chart model and approximation: Fix $r > 0$ and write $B_r := \{v \in \mathbb{R}^d : |v| \leq r\}$. Assume $\Psi : B_r \rightarrow \mathcal{M}$ is a C^2 embedding onto $\mathcal{M}_r := \Psi(B_r)$ with $\Psi(0) = \tilde{\mu}$, $D\Psi(0) = N$, and $\text{Lip}(\Psi) \leq L_\Psi$ on B_r . Assume the second-order residual bound

$$\|\Psi(v) - (\tilde{\mu} + Nv)\| \leq \frac{\kappa_\Psi}{2} |v|^2, \quad v \in B_r, \quad (30)$$

and a quadratic control on the Jacobian factor $J(v)$ defined by $d\text{Vol}_{\mathcal{M}}(\Psi(v)) = J(v) dv$:

$$|\log J(v)| \leq \frac{\kappa_J}{2} |v|^2, \quad v \in B_r, \quad (31)$$

Let $\bar{\Psi} : \mathbb{R}^d \rightarrow \mathcal{M}$ be a measurable extension of Ψ such that $\bar{\Psi}(v) \in \mathcal{M}_r$ iff $v \in B_r$ (e.g., map $v \notin B_r$ to any fixed point in $\mathcal{M} \setminus \mathcal{M}_r$), and define the approximate conditioned law

$$\hat{P}_{\text{cond}} := \bar{\Psi}_{\#} Q_T. \quad (32)$$

Tail quantities: Define

$$\varepsilon_P := P_{\text{cond}}(\mathcal{M} \setminus \mathcal{M}_r), \quad \varepsilon_Q := Q_T(\mathbb{R}^d \setminus B_r),$$

and the corresponding tail second moments (w.r.t. $\tilde{\mu}$)

$$\begin{aligned} \tau_P(r) &:= \left(\mathbb{E}[\|Y - \tilde{\mu}\|^2 \mathbf{1}_{\{Y \notin \mathcal{M}_r\}}] \right)^{1/2}, \quad (Y \sim P_{\text{cond}}), \\ \tau_{\hat{P}}(r) &:= \left(\mathbb{E}[\|\hat{Y} - \tilde{\mu}\|^2 \mathbf{1}_{\{\hat{Y} \notin \mathcal{M}_r\}}] \right)^{1/2}, \quad (\hat{Y} \sim \hat{P}_{\text{cond}}). \end{aligned}$$

Define the curvature/volume mismatch exponent

$$\eta_r := \frac{\|\Omega\| \kappa_\Psi}{2} (\|\delta\| + r) r^2 + \frac{\|\Omega\| \kappa_\Psi^2}{8} r^4 + \frac{\kappa_J}{2} r^2. \quad (33)$$

Theorem IV.1 (W_2 stability of surface-measure conditioning under chart linearization). *Under the assumptions above,*

$$\begin{aligned} W_2(P_{\text{cond}}, \hat{P}_{\text{cond}}) &\leq \tau_P(r) + \tau_{\hat{P}}(r) + L_\Psi r (\sqrt{\varepsilon_P} + \sqrt{\varepsilon_Q}) \\ &\quad + 2L_\Psi r \sqrt{\tanh(\eta_r)}. \end{aligned} \quad (34)$$

Lemma IV.2 (Truncation bound). *Let P be a probability measure on a subset of \mathbb{R}^m with finite second moment. Let A be measurable with $P(A) = 1 - \varepsilon \in (0, 1]$, and let $P(\cdot | A)$ be the conditional law. Fix any $x_0 \in A$ and define $R_A := \sup_{x \in A} \|x - x_0\|$ (possibly $+\infty$). Then*

$$\begin{aligned} W_2(P, P(\cdot | A)) &\leq \left(\mathbb{E}[\|X - x_0\|^2 \mathbf{1}_{A^c}] \right)^{1/2} \\ &\quad + R_A \sqrt{\varepsilon}, \quad (X \sim P). \end{aligned}$$

Proof. Define the auxiliary measure $\tilde{P} := (1 - \varepsilon) P(\cdot | A) + \varepsilon \delta_{x_0}$. Couple P with \tilde{P} by keeping the mass on A fixed and sending all A^c mass to x_0 . By (3), this gives

$$W_2(P, \tilde{P}) \leq \left(\mathbb{E}[\|X - x_0\|^2 \mathbf{1}_{A^c}] \right)^{1/2}.$$

Next, couple \tilde{P} to $P(\cdot | A)$ by moving the extra point mass $\varepsilon \delta_{x_0}$ into A according to $P(\cdot | A)$; the cost is at most $R_A \sqrt{\varepsilon}$. The claim follows by the triangle inequality. \square

Lemma IV.3 (Diameter-TV control of W_2 on bounded support). *Let p, q be probability measures supported on a set $S \subset \mathbb{R}^d$ with $\text{diam}(S) := \sup_{u, v \in S} \|u - v\| < \infty$. Then*

$$\begin{aligned} W_2(p, q) &\leq \text{diam}(S) \sqrt{\text{TV}(p, q)}, \\ \text{TV}(p, q) &:= \frac{1}{2} \int |dp - dq|. \end{aligned}$$

Proof. Let γ be a maximal coupling of (p, q) so that $\gamma\{(U, V) : U \neq V\} = \text{TV}(p, q)$ [22]. On $\{U = V\}$ the cost is 0, and on $\{U \neq V\}$ we have $\|U - V\| \leq \text{diam}(S)$. Thus $\mathbb{E}_\gamma \|U - V\|^2 \leq \text{diam}(S)^2 \text{TV}(p, q)$, and the claim follows by infimizing over couplings. \square

Lemma IV.4 (TV control from a likelihood-ratio bound). *Let p, q be probability measures with $p \ll q$ and*

$$\frac{dp}{dq} \in [\Lambda^{-1}, \Lambda] \quad q\text{-a.e.},$$

for some $\Lambda \geq 1$. Then

$$\text{TV}(p, q) \leq \frac{\Lambda - 1}{\Lambda + 1}.$$

Proof. Let $h := dp/dq$, $a := \Lambda^{-1}$, and $b := \Lambda$. Then

$$\begin{aligned} \text{TV}(p, q) &= \frac{1}{2} \mathbb{E}_q[|h - 1|], \quad \mathbb{E}_q[h] = 1, \\ h &\in [a, b] \quad q\text{-a.e.} \end{aligned}$$

Since $x \mapsto |x - 1|$ is convex on $[a, b]$, for $x \in [a, b]$,

$$|x - 1| \leq \frac{b - x}{b - a} |a - 1| + \frac{x - a}{b - a} |b - 1|.$$

Applying this with $x = h$ and taking \mathbb{E}_q ,

$$\begin{aligned} \mathbb{E}_q[|h - 1|] &\leq \frac{b - \mathbb{E}_q[h]}{b - a} |a - 1| + \frac{\mathbb{E}_q[h] - a}{b - a} |b - 1| \\ &= \frac{2(1 - a)(b - 1)}{b - a}. \end{aligned}$$

Hence

$$\text{TV}(p, q) \leq \frac{(1 - a)(b - 1)}{b - a} = \frac{\Lambda - 1}{\Lambda + 1}. \quad \square$$

Proof of Theorem IV.1. Recall P_{cond} from (9), Q_T from (28), and $\hat{P}_{\text{cond}} = \bar{\Psi}_{\#} Q_T$ from (32). Let $\mathcal{M}_r = \Psi(B_r)$, and define truncations

$$P_{\text{cond}}^{(r)} := P_{\text{cond}}(\cdot | \mathcal{M}_r), \quad \hat{P}_{\text{cond}}^{(r)} := \hat{P}_{\text{cond}}(\cdot | \mathcal{M}_r).$$

We first separate tail and interior contributions. By the triangle inequality,

$$\begin{aligned} W_2(P_{\text{cond}}, \hat{P}_{\text{cond}}) &\leq W_2(P_{\text{cond}}, P_{\text{cond}}^{(r)}) + W_2(P_{\text{cond}}^{(r)}, \hat{P}_{\text{cond}}^{(r)}) \\ &\quad + W_2(\hat{P}_{\text{cond}}^{(r)}, \hat{P}_{\text{cond}}). \end{aligned} \quad (35)$$

The two outer terms are tail terms. Applying Lemma IV.2 with $P = P_{\text{cond}}$, $A = \mathcal{M}_r$, and $x_0 = \tilde{\mu} \in \mathcal{M}_r$ gives

$$W_2(P_{\text{cond}}, P_{\text{cond}}^{(r)}) \leq \tau_P(r) + L_\Psi r \sqrt{\varepsilon_P}, \quad (36)$$

since $\sup_{x \in \mathcal{M}_r} \|x - \tilde{\mu}\| \leq L_\Psi r$. Applying the same lemma to \hat{P}_{cond} yields

$$W_2(\hat{P}_{\text{cond}}^{(r)}, \hat{P}_{\text{cond}}) \leq \tau_{\hat{P}}(r) + L_\Psi r \sqrt{\varepsilon_Q}, \quad (37)$$

because $\widehat{P}_{\text{cond}}(\mathcal{M} \setminus \mathcal{M}_r) = Q_T(\|V\| > r) = \varepsilon_Q$.

For the interior term, use that $\Psi : B_r \rightarrow \mathcal{M}_r$ is bijective and pull both truncated laws back to B_r . Define unnormalized densities

$$\tilde{p}(v) := \varphi_{\mu, \Sigma}(\Psi(v)) J(v), \quad \tilde{q}(v) := \varphi_{\mu, \Sigma}(\tilde{\mu} + Nv).$$

Let $p_r := \tilde{p} / \int_{B_r} \tilde{p}$ and $q_r := \tilde{q} / \int_{B_r} \tilde{q}$. Then $P_{\text{cond}}^{(r)} = \Psi_{\#} p_r$ and $\widehat{P}_{\text{cond}}^{(r)} = \Psi_{\#} q_r$, so by (4)

$$W_2(P_{\text{cond}}^{(r)}, \widehat{P}_{\text{cond}}^{(r)}) \leq L_{\Psi} W_2(p_r, q_r). \quad (38)$$

Since p_r, q_r are supported on B_r and $\text{diam}(B_r) \leq 2r$, Lemma IV.3 gives $W_2(p_r, q_r) \leq 2r \sqrt{\text{TV}(p_r, q_r)}$, hence

$$W_2(P_{\text{cond}}^{(r)}, \widehat{P}_{\text{cond}}^{(r)}) \leq 2L_{\Psi} r \sqrt{\text{TV}(p_r, q_r)}. \quad (39)$$

It remains to bound $\text{TV}(p_r, q_r)$. Write $x(v) := \tilde{\mu} + Nv$ and $e(v) := \Psi(v) - x(v)$. By (30), $\|e(v)\| \leq \frac{\kappa_{\Psi}}{2} \|v\|^2 \leq \frac{\kappa_{\Psi}}{2} r^2$ on B_r . Since $\log \varphi_{\mu, \Sigma}(x) = \text{const} - \frac{1}{2}(x - \mu)^{\top} \Omega (x - \mu)$,

$$\begin{aligned} |\log \varphi_{\mu, \Sigma}(\Psi(v)) - \log \varphi_{\mu, \Sigma}(x(v))| &\leq \frac{\|\Omega\| \kappa_{\Psi}}{2} (\|\delta\| + r) r^2 \\ &\quad + \frac{\|\Omega\| \kappa_{\Psi}^2}{8} r^4. \end{aligned}$$

Together with (31), this yields $|\log \tilde{p}(v) - \log \tilde{q}(v)| \leq \eta_r$ on B_r . Hence $e^{-\eta_r} \tilde{q} \leq \tilde{p} \leq e^{\eta_r} \tilde{q}$ on B_r , and after normalization $\frac{p_r(v)}{q_r(v)} \in [e^{-2\eta_r}, e^{2\eta_r}]$. Lemma IV.4 then gives

$$\text{TV}(p_r, q_r) \leq \frac{e^{2\eta_r} - 1}{e^{2\eta_r} + 1} = \tanh(\eta_r). \quad (40)$$

Combining (39) and (40),

$$W_2(P_{\text{cond}}^{(r)}, \widehat{P}_{\text{cond}}^{(r)}) \leq 2L_{\Psi} r \sqrt{\tanh(\eta_r)}. \quad (41)$$

Finally, inserting (36), (41), and (37) into (35) gives (34). \square

Gaussian specialization: Recall $Q_T = \mathcal{N}(m_T, \Sigma_T)$ on \mathbb{R}^d from (29). Define $\varepsilon_Q := Q_T(\mathbb{R}^d \setminus B_r) = \mathbb{P}(\|V\| > r)$ for $V \sim Q_T$. As in (27), Gaussian concentration gives (with $\lambda_{\max, T} := \|\Sigma_T\|_{\text{op}}$)

$$\varepsilon_Q \leq \exp\left(-\frac{1}{2}\left(\frac{r - \|m_T\|}{\sqrt{\lambda_{\max, T}}} - \sqrt{d}\right)_+^2\right).$$

The truncation moment term $\tau_{\widehat{P}}(r)$ can be bounded in terms of Q_T and chart Lipschitzness: since $\|\Psi(v) - \tilde{\mu}\| \leq L_{\Psi} \|v\|$ on B_r and $\widehat{P}_{\text{cond}} = \Psi_{\#} Q_T$,

$$\begin{aligned} \tau_{\widehat{P}}(r) &:= \left(\mathbb{E}[\|\hat{Y} - \tilde{\mu}\|^2 \mathbf{1}_{\{\hat{Y} \notin \mathcal{M}_r\}}]\right)^{1/2} \\ &\leq L_{\Psi} \left(\mathbb{E}[\|V\|^2 \mathbf{1}_{\{\|V\| > r\}}]\right)^{1/2}. \end{aligned}$$

Here \hat{Y} denotes a sample from $\widehat{P}_{\text{cond}}$. A convenient fully explicit bound follows from Cauchy–Schwarz:

$$\mathbb{E}[\|V\|^2 \mathbf{1}_{\{\|V\| > r\}}] \leq (\mathbb{E}\|V\|^4)^{1/2} \varepsilon_Q^{1/2},$$

where $\mathbb{E}\|V\|^4$ has the same closed form as (26) with (δ, Σ) replaced by (m_T, Σ_T) :

$$\begin{aligned} \mathbb{E}\|V\|^4 &= \|m_T\|^4 + 2\|m_T\|^2 \text{tr} \Sigma_T + 4m_T^{\top} \Sigma_T m_T \\ &\quad + (\text{tr} \Sigma_T)^2 + 2\|\Sigma_T\|_F^2. \end{aligned}$$

Thus $\tau_{\widehat{P}}(r)$ admits an explicit upper bound in terms of $(m_T, \Sigma_T, L_{\Psi}, r)$ and ε_Q . The remaining tail quantities $(\varepsilon_P, \tau_P(r))$ are geometric (they quantify how much of the true conditioned law lies outside the chart image \mathcal{M}_r).

Interpretation and numerical illustration: Equation (34) splits conditioning error into (i) tail/truncation penalties and (ii) interior in-chart distortion. The tail terms

$$\tau_P(r) + \tau_{\widehat{P}}(r) + L_{\Psi} r (\sqrt{\varepsilon_P} + \sqrt{\varepsilon_Q})$$

measure mass outside $\mathcal{M}_r = \Psi(B_r)$ under the true law P_{cond} and the approximation $\widehat{P}_{\text{cond}}$. The interior term

$$2L_{\Psi} r \sqrt{\tanh(\eta_r)}$$

captures chart-induced likelihood distortion, where η_r combines second-order chart residual and Jacobian distortion weighted by precision $\|\Omega\|$. Thus, high-confidence regimes can amplify small geometric errors even when truncation is mild. For affine manifolds with exact charts ($\kappa_{\Psi} = \kappa_J = 0$), $\eta_r = 0$ and only truncation remains. Figure 2 illustrates this transition: near-local regimes show close agreement, whereas larger spread introduces mode/variance mismatch and then tail-dominated failure.

V. NUMERICAL EXPERIMENTS

A. 2-D circle benchmark

Goals and setup: We consider $\mathcal{M} = \{x \in \mathbb{R}^2 : \|x\| = R\}$ with curvature $\kappa = 1/R$, reach $\rho = R$, and $X \sim \mathcal{N}(\mu, \Sigma)$ where $\mu = (R + \delta, 0)$. The baseline uses isotropic covariance $\Sigma = \sigma^2 I_2$ with $\delta = 0.2$. We then add two stress tests to assess robustness: (i) anisotropic covariance, $\Sigma = \text{diag}(\sigma_n^2, \sigma_t^2)$ in the normal/tangential frame, and (ii) offset sweeps in δ/R . These tests probe the computable diagnostics in Theorem III.1, especially the roles of $\sqrt{\|\Sigma\|_{\text{op}}}$ and the tail-leakage term ε . For marginalization, the exact map is $g(x) = Rx/\|x\|$, and the approximation is tangent projection plus normalization at $\tilde{\mu} = g(\mu) = (R, 0)$. For conditioning, we compare surface-measure conditioning on \mathcal{M} against tangent-line conditioning followed by retraction.

Quantitative sweep: Figure 3 sweeps $\sigma/R \in [0.02, 1.2]$ for $R \in \{0.5, 1, 2\}$ and reports (i) variance ratio $\rho = \text{Var}_{\text{in}}(\theta)/\text{Var}_{\text{exact}}(\theta)$, (ii) coverage of a nominal 95% interval, and (iii) normalized theoretical/empirical W_2 diagnostics for marginalization. Panel (a) shows ρ crossing below 1 near $\sigma/R = 1/6$; panel (b) shows corresponding coverage degradation outside that regime; panel (c) uses $\sqrt{\|\Sigma\|_{\text{op}}}/R$ and compares empirical W_2 proxies against tightened theoretical W_2 bounds with data-calibrated C_{tail} (90% quantile pre-fit plus a strict upper-envelope safeguard: $C_{\text{tail}} = 0.137$ for $R = 0.5$, 0.165 for $R = 1$, and 0.183 for $R = 2$), so the bound remains above the empirical proxy while preserving the failure-onset trend.

Anisotropic Σ and offset sweeps: Figure 4 extends the circle benchmark along two complementary axes. Panel (a) varies anisotropy $\eta := \sigma_n/\sigma_t \in \{0.5, 1, 2, 4\}$ and replots calibration against the spectral scale $\sqrt{\|\Sigma\|_{\text{op}}}/R$. The transition remains aligned across anisotropy levels, supporting $\|\Sigma\|_{\text{op}}$

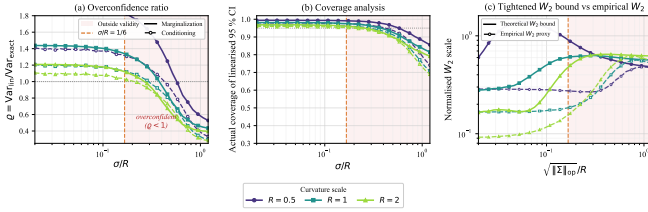


Fig. 3: Circle sweep ($\delta = 0.2$) over σ/R : (a) variance ratio $\rho = \text{Var}_{\text{lin}}/\text{Var}_{\text{exact}}$, (b) realized 95% coverage, and (c) normalized diagnostics on $\sqrt{\|\Sigma\|_{\text{op}}}/R$: tightened theoretical W_2 bound (data-calibrated C_{tail} with strict upper-envelope safeguard) and empirical W_2 proxy. Dashed line marks $\sigma/R = 1/6$; colors indicate $R \in \{0.5, 1, 2\}$.

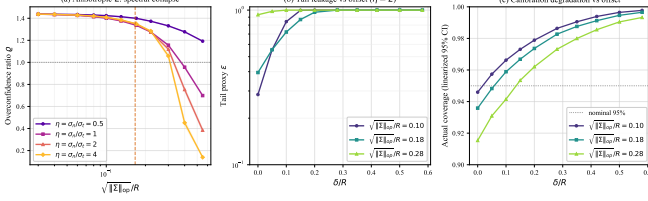


Fig. 4: Circle generality stress tests: (a) anisotropic sweep ($\eta = \sigma_n/\sigma_t$) versus $\sqrt{\|\Sigma\|_{\text{op}}}/R$, (b) tail proxy ε versus offset δ/R , and (c) coverage degradation versus δ/R .

as an effective diagnostic variable in the bound. Panels (b)–(c) fix anisotropy and sweep δ/R : as offset increases, the tail proxy ε rises rapidly and coverage degrades even at fixed curvature/noise scale, revealing a second failure axis beyond curvature-only effects. This behavior matches the decomposition in Theorem III.1, where local distortion and nonlocal leakage contribute separately.

B. Planar pushing: diagnostics in a contact-rich task

Setup and covariance models: We use the standard 2-D planar-pushing benchmark from constrained GTSAM/InCOpt to evaluate covariance extraction under hard contact constraints [2, 3]. A rectangular box state $x_k = (p_{x,k}, p_{y,k}, \theta_k) \in \mathbb{R}^2 \times \mathbb{S}^1$ is pushed by a circular probe whose center follows a known deterministic path; the probe is assumed to remain in contact with the box boundary at every step, encoded as a per-pose contact factor $c_k(x_k) = 0$. Odometry provides relative-pose measurements with wrapped-angle noise, $u_k = x_{k+1} - x_k + \varepsilon_k$, $\varepsilon_k \sim \mathcal{N}(0, Q)$, $Q = \text{diag}(0.03^2, 0.03^2, 0.01^2)$. We use $r_p = 0.1$ m, $(w, h) = (0.2, 1.0)$ m, and $n_{\text{steps}} = 50$. The constrained mean is obtained from constrained least squares:

$$\min_{x_{1:n}} \sum_{k=0}^{n-1} \|r_k(x)\|_{Q^{-1}}^2 \quad \text{s.t.} \quad c_k(x_k) = 0, \quad \forall k,$$

with $r_k(x) := x_{k+1} - (x_k + u_k)$. Linearizing about the optimized trajectory, we form the (unconstrained) Gauss–Newton information $F \approx H^T W^{-1} H$ with $W = \text{blkdiag}(Q, \dots, Q)$, giving $\Sigma_{\text{unc}} = F^{-1}$, and compute the constrained covariance by conditioning onto the linearized contact constraints: $\Sigma_{\text{con}} = N(N^T F N)^{-1} N^T$, where $N \in \text{null}(S^T)$ spans the tangent directions of the constraint manifold.

Aggregate covariance reduction: Across 49 optimized timesteps, equality constraints are satisfied to numerical precision. Table I reports representative timesteps: the constrained

TABLE I: Quantitative covariance metrics for planar pushing at timesteps

k	$\text{tr}(\Sigma_{xy})$		$\lambda_{\max}(\Sigma_{xy})$		Red. (%)	$\ \Delta\Sigma_{xy}\ _F$
	Unc.	Con.	Unc.	Con.		
1	0.0018	0.0009	0.0009	0.0009	50.5	0.0009
13	0.0234	0.0105	0.0117	0.0105	55.3	0.0118
25	0.0450	0.0190	0.0225	0.0190	57.8	0.0228
37	0.0666	0.0278	0.0333	0.0278	58.2	0.0337
49	0.0882	0.0377	0.0441	0.0377	57.3	0.0446

xy -marginal covariance trace is reduced by 50.5% at $k = 1$ and 57.3% at $k = 49$, with a peak reduction of 58.2% at $k = 37$. These values establish a trajectory-level baseline before the Monte Carlo calibration diagnostics.

Trajectory-wide diagnostics: To move beyond single-pose checks, we evaluate diagnostics at every timestep. Let $c_k(x) = 0$ be the contact constraint at step k , linearized at \hat{x}_k . With N_k spanning $\text{null}(\nabla c_k(\hat{x}_k)^T)$, we define

$$\hat{\kappa}_k := \frac{\|N_k^T \nabla^2 c_k(\hat{x}_k) N_k\|_{\text{op}}}{\|\nabla c_k(\hat{x}_k)\|}, \quad \hat{\rho}_k := \frac{1}{\max(\hat{\kappa}_k, \epsilon_\kappa)},$$

as curvature/reach proxies ($\epsilon_\kappa = 10^{-8}$ for numerical stability), and the uncertainty spread

$$s_k := \sqrt{\|\Sigma_{\text{unc},k}\|_{\text{op}}}.$$

At each k , we compare tangent-plane covariance $\Sigma_{\text{lin},k} := \Pi_k \Sigma_{\text{unc},k} \Pi_k^T$ against Monte Carlo covariance $\Sigma_{\text{MC},k}$ after exact nonlinear projection, via

$$\varrho_k^{\text{MC}} := \frac{\text{tr}(\Sigma_{\text{MC},xy,k})}{\text{tr}(\Sigma_{\text{lin},xy,k})}, \quad \Delta_k := \frac{\|\Sigma_{\text{MC},xy,k} - \Sigma_{\text{lin},xy,k}\|_F}{\|\Sigma_{\text{lin},xy,k}\|_F}.$$

Figure 5 shows a non-uniform failure profile over time. Larger mismatch co-occurs with larger locality-pressure indicators ($s_k/\hat{\rho}_k$), consistent with the tail-leakage interpretation in Theorem III.1. The largest mismatch occurs at $k = 13$ ($\varrho_{13}^{\text{MC}} = 2.162$, locality index $s_{13}/\hat{\rho}_{13} = 0.119$); the median trajectory-wide mismatch is $\text{median}(\varrho_k^{\text{MC}}) = 1.557$ with median relative Frobenius discrepancy $\text{median}(\Delta_k) = 0.525$.

Directional uncertainty stress test: Isotropic scaling $\Sigma \mapsto \alpha^2 \Sigma$ obscures direction-specific failures. At the terminal pose k^* , with local unit normal \hat{n} , define $A(\alpha_n, \alpha_t) := \alpha_t(I - \hat{n}\hat{n}^T) + \alpha_n \hat{n}\hat{n}^T$ and $\Sigma(\alpha_n, \alpha_t) := A \Sigma_{\text{unc},k^*} A^T$. We compare isotropic (α, α) , normal-only $(\alpha, 1)$, and tangential-only $(1, \alpha)$ sweeps. Figure 6 shows a clear asymmetry for $\alpha \geq 1$: normal-direction inflation causes the largest calibration and covariance mismatch.

VI. DISCUSSION

Practical validity test for robotics estimation: The bounds can be implemented as a runtime gate in factor-graph pipelines. At each linearization point, compute the curvature-load indicator $s_c := \kappa \sqrt{\|\Sigma\|_{\text{op}}}$ and offset indicator $s_\delta := \delta/\rho$. For marginalization, evaluate (26) and (27) with (ρ, κ, r) to obtain local-distortion and tail-leakage terms in (13). For conditioning, combine computable $(\varepsilon_Q, \tau_{\hat{P}}(r), \eta_r)$ with sample-based or certified estimates of $(\varepsilon_P, \tau_P(r))$. Single-chart tangent-linearized inference is retained only when the predicted bound is below an application tolerance and both

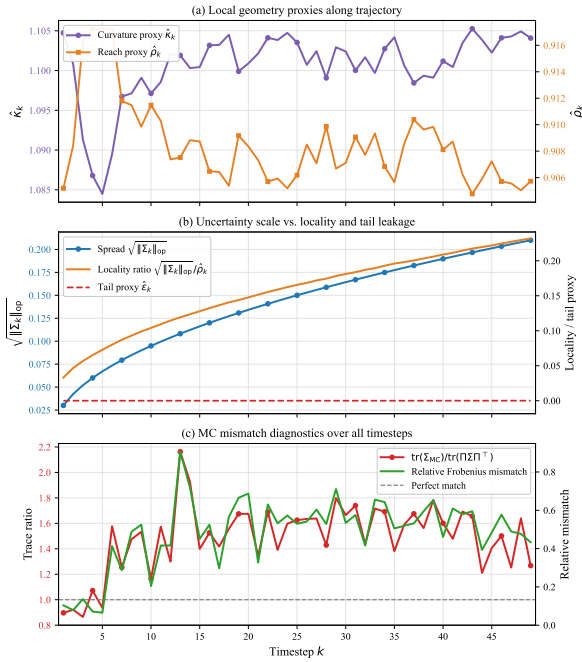


Fig. 5: Trajectory-wide planar-pushing diagnostics: (a) curvature/reach proxies $(\hat{\kappa}_k, \hat{\rho}_k)$, (b) spread s_k and locality indicator $s_k/\hat{\rho}_k$, (c) Monte Carlo mismatch $(\theta_k^{MC}, \Delta_k)$.

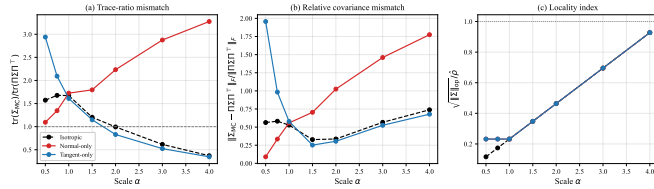


Fig. 6: Directional scaling at the terminal planar-pushing pose: isotropic, normal-only, and tangential-only covariance inflation.

indicators remain in a calibrated safe range. Otherwise, the solver escalates in stages to iterated relinearization [23], multi-chart updates [24, 25], and finally sample-based inference [26, 27] when tail leakage or shape mismatch persists.

Limitations: The constants are conservative because the proofs use general coupling/concentration inequalities rather than manifold-specific transport constructions, so theorem-level bounds can overestimate empirical error in low-curvature regimes. The analysis also assumes C^2 manifolds with positive reach and does not cover corners, self-intersections, or singular geometries. Extending guarantees to piecewise-smooth contact manifolds and iterative multi-chart updates remains an important direction for future work.

VII. CONCLUSION

We presented explicit non-asymptotic W_2 stability guarantees for tangent-linearized Gaussian inference on smooth manifolds, with local geometric and nonlocal tail terms for both projection marginalization and surface-measure conditioning. Experiments on a circle benchmark and planar pushing support a calibration transition near $\sqrt{\|\Sigma\|_{op}}/R \approx 1/6$ and highlight normal-direction uncertainty as the primary driver of mismatch in contact-rich settings. Operationally, the

bounds and diagnostics provide a principled trigger for when single-chart linearization is adequate and when escalation to multi-chart or sample-based inference is warranted.

REFERENCES

- [1] T. D. Barfoot, *State estimation for robotics*. Cambridge University Press, 2024.
- [2] M. Qadri, P. Sodhi, J. G. Mangelson, F. Dellaert, and M. Kaess, “Incopt: Incremental constrained optimization using the bayes tree,” in *IEEE/RSJ IROS*, 2022.
- [3] M. Kaess, H. Johannsson, R. Roberts, V. Ila, J. Leonard, and F. Dellaert, “isam2: Incremental smoothing and mapping with fluid relinearization and incremental variable reordering,” in *IEEE/RSJ ICRA*, 2011.
- [4] I. A. Şucan and S. Chitta, “Motion planning with constraints using configuration space approximations,” in *IEEE/RSJ IROS*, 2012.
- [5] R. M. Eustice, H. Singh, and J. J. Leonard, “Exactly sparse delayed-state filters for view-based slam,” *IEEE Transactions on Robotics*, 2006.
- [6] Z. C. Guo, J. R. Forbes, and T. D. Barfoot, “Marginalizing and conditioning gaussians onto linear approximations of smooth manifolds with applications in robotics,” in *IEEE/RSJ ICRA*, 2025, pp. 2606–2612.
- [7] M. Kaess and F. Dellaert, “Covariance recovery from a square root information matrix for data association,” *Robotics and Autonomous Systems*, 2009.
- [8] F. Wang and A. E. Gelfand, “Directional data analysis under the general projected normal distribution,” *Statistical methodology*, 2013.
- [9] D. Hernandez-Stumpfhauser, F. J. Breidt, and M. J. van der Woerd, “The general projected normal distribution of arbitrary dimension: Modeling and bayesian inference,” *Bayesian Analysis*, 2017.
- [10] G. Bourmaud, R. Mégret, M. Arnaudon, and A. Giremus, “Continuous-discrete extended kalman filter on matrix lie groups using concentrated gaussian distributions,” *Journal of Mathematical Imaging and Vision*, 2015.
- [11] S. Bonnabre, P. Martin, and E. Salaün, “Invariant extended kalman filter: theory and application to a velocity-aided attitude estimation problem,” in *IEEE CDC*, 2009.
- [12] P. van Goor, T. Hamel, and R. Mahony, “Equivariant filter (eqf),” *IEEE Transactions on Automatic Control*, 2022.
- [13] C. Villani *et al.*, *Optimal transport: old and new*. Springer, 2008.
- [14] G. Peyré, M. Cuturi *et al.*, “Computational optimal transport: With applications to data science,” *Foundations and Trends® in Machine Learning*, 2019.
- [15] P.-A. Absil, R. Mahony, and R. Sepulchre, *Optimization Algorithms on Matrix Manifolds*. Princeton University Press, 2008.
- [16] V. M. Panaretos and Y. Zemel, “Statistical aspects of wasserstein distances,” *Annual review of statistics and its application*, 2019.
- [17] H. Federer, “Curvature measures,” *Transactions of the American Mathematical Society*, 1959.
- [18] J. M. Lee, *Riemannian manifolds: an introduction to curvature*. Springer Science & Business Media, 2006.
- [19] J.-D. Boissonnat, S. Kachanovich, and M. Wintraecken, “Triangulating submanifolds: an elementary and quantified version of whitney’s method,” *Discrete & Computational Geometry*, 2021.
- [20] P. Niyogi, S. Smale, and S. Weinberger, “Finding the homology of submanifolds with high confidence from random samples,” *Discrete & Computational Geometry*, 2008.
- [21] R. Vershynin, “High-dimensional probability,” 2009.
- [22] H. Thorisson, “Coupling, stationarity, and regeneration,” *Probability and its Applications*, 2000.
- [23] B. M. Bell and F. W. Cathey, “The iterated kalman filter update as a gauss-newton method,” *IEEE Transactions on Automatic Control*, 1993.
- [24] J. Česić, I. Marković, and I. Petrović, “Mixture reduction on matrix lie groups,” *IEEE Signal Processing Letters*, 2017.
- [25] J. C. Nascimento, J. G. Silva, J. S. Marques, and J. M. Lemos, “Manifold learning for object tracking with multiple nonlinear models,” *IEEE Transactions on Image Processing*, 2014.
- [26] N. J. Gordon, D. J. Salmond, and A. F. Smith, “Novel approach to nonlinear/non-gaussian bayesian state estimation,” in *IEE Proceedings F (Radar and Signal Processing)*, 1993.
- [27] M. C. Koval, M. Klingensmith, S. S. Srinivasa, N. S. Pollard, and M. Kaess, “The manifold particle filter for state estimation on high-dimensional implicit manifolds,” in *IEEE/RSJ ICRA*, 2017.